International Journal of Heat and Mass Transfer 52 (2009) 2690–2703

Contents lists available at ScienceDirect

International Journal of Heat and Mass Transfer

journal homepage: www.elsevier.com/locate/ijhmt

# Simulation of airflow in one- and two-room enclosures containing a fire source

G.M. Stavrakakis, N.C. Markatos *

*Computational Fluid Dynamics Unit, School of Chemical Engineering, National Technical University of Athens (N.T.U.A.), Iroon Polytechniou 9, Gr-15780 Athens, Greece*

ARTICLE INFO

*Article history:*
Received 15 March 2007
Available online 14 February 2009

*Keywords:*
Computational Fluid Dynamics
Compartment fires
Buoyant–turbulent flow

ABSTRACT

In this study, the airflow in a room that contains a heat source is simulated numerically. The flow is considered turbulent and buoyant. The results of the mathematical model are validated with available experimental data at specific locations in the domain. A simple geometry is adopted, consisting of a room with a door that plays the role of both inlet–outlet for the fluid (air). At the centre of the room a methane burner is placed to serve as a heat source. The problem is simulated using two turbulence models, the well-known standard $k$–$\varepsilon$ model and the RNG $k$–$\varepsilon$ model, both modified to account for buoyancy effects on turbulence. The burner is considered as a volumetric heat source. It is concluded that the fire plume development as well as the distributions of velocity and temperature are reasonably well predicted. Following this conclusion, both models are also applied to a different, more complex geometry that consisted of two rooms communicating via a door, while the heat source was placed in the first room. Unfortunately, there are no experimental data to compare with for this case, but the results appear plausible. Finally, important design factors, such as mass flow rates and neutral-plane heights, are calculated utilizing the CFD results, and are compared with those obtained by well-known empirical correlations. It is concluded that the bi-directional flow existing through the burning-room vent is similarly predicted by both turbulence models; the RNG $k$–$\varepsilon$ model leading to higher, and more accurate predictions of temperature variations within the hot upper layer, at least for the single-room case.



## 1. Introduction

The modelling of fire spread within a building presents a formidable challenge for mathematicians, physicists and engineers. Fire, which is conventionally defined as uncontrolled flame spread, is arguably among the most complex phenomena considered in combustion science. It embraces nearly all of the effects found in subsonic chemically reacting flows. Fluid dynamics, kinetics, radiation, and in many cases multi-phase flow effects are linked together to provide an extremely complex physical and chemical phenomenon [1–3].

Typical values of Reynolds number for airflow induced by fire in enclosures are of the order of $10^5$ [4], while the buoyancy force due to density differences between hot and ambient air is usually much greater than both the inertial and the viscous ones [3,5], i.e., the expected airflow induced by thermal sources inside an enclosure is strongly buoyant and turbulent. The influence of buoyancy forces on the airflow structure (thermal plume development, smoke spreading, etc.) depends primarily on the ventilation grade of the enclosure containing the fire-source [6], e.g., whether the enclosure is unventilated, mechanically ventilated (controllable) or naturally ventilated [6,7]. In the latter case, it is crucial to evaluate the effects of the external wind forces, as compared to the buoyancy forces, on the indoor airflow, in order to develop a mathematical model to describe the phenomenon. This can be achieved using the Archimedes number, as for example in [8], according to which buoyancy or wind forces prevail when Ar >> 1 or Ar << 1, respectively [9]. In compartment fires, such as that in the present study, the Archimedes number is far above unity, and the flow is buoyancy dominated. The objective of fire-safety systems design is mainly the extraction of smoke at a rate sufficient to prevent the smoke layer from descending to an occupied zone. Thus, the quantification of the smoke layer properties (temperature, concentration of combustion products, etc.), of the mass flow rates through the opening, as well as of the neutral-plane height [3,10] is the prime desideratum.

The most widely-used models to quantify the fire-driven flow field are the so-called zone models and the field, or Computational Fluid Dynamics (CFD), models. The former approach is based on the division of the space under consideration into different distinctive zones, each of which can be described by a simple set of parameters and empirical laws. The parameters that represent physical quantities are averaged over each zone, while the conservation conditions at the boundaries between different regions, together with global conservation laws, lead to a system of equations which determines the parameters of interest [3]. These models

* Corresponding author. Tel.: +30 210772 3126; fax: +30 210772 3228.
*E-mail addresses:* gstavr@mail.ntua.gr (G.M. Stavrakakis), N.Markatos@ntua.gr (N.C. Markatos).

0017-9310/$ - see front matter © 2009 Elsevier Ltd. All rights reserved.
doi:10.1016/j.ijheatmasstransfer.2007.10.046

**Nomenclature**

| | |
|---|---|
| $A$ | burning-room opening area ($m^2$) |
| $A_r$ | Archimedes number |
| $a$ | numerical coefficients |
| $C_0$ | inflow coefficient |
| $C_d$ | drag coefficient |
| $C_1$, $C_2$, $C_3$, $C_\mu$ | empirical constants in the turbulence models |
| Grashof | Grashof number |
| $g$ | gravitational acceleration ($m/s^2$) |
| $G_B$ | buoyancy source/sink term |
| $H$ | opening height (m) |
| $H_h$ | neutral-plane height in the adjacent room (m) |
| $h$ | enthalpy (J/kg) |
| $k$ | turbulence kinetic energy ($m^2/s^2$) |
| $\dot{m}_a$ | mass-inflow rate (kg/s) |
| $\dot{m}_g$ | mass-outflow rate (kg/s) |
| $\dot{m}_{g1}$ | mass-ouflow rate between neutral-plane heights of the burning and the adjacent room (kg/s) |
| $\dot{m}_{g2}$ | mass-outflow rate above the adjacent-room neutral-plane height (kg/s) |
| $\dot{m}_{fuel}$ | fuel burning rate (kg/s) |
| $N$ | neutral-plane height through the doorway of the burning room (m) |
| $P_k$ | turbulence kinetic energy generation term |
| $\dot{q}'''$ | volumetric heat-release rate ($J/(m^3 s)$) |
| Reynolds | Reynolds number |
| $R$ | rate-of-strain term |
| RES | absolute residual |
| $S$ | mean rate of strain |
| $S_\varphi$ | source term in the general transport equation |
| $S_h$ | enthalpy source term (J/(kg s)) |
| $t$ | time (s) |
| $T$ | temperature (K) |
| $T_a$ | surrounding gas temperature in the one-room case (K) |
| $T_{a1}$ | temperature of the cold layer in the adjacent room (K) |
| $T_{a2}$ | temperature of the hot layer in the adjacent room (K) |
| $T_{i_{burn}}$ | temperature stored in the $i$-th cell within the burning room (K) |
| $T_r$ | temperature in the burning room (K) |
| $T_{ref}$ | reference temperature (K) |
| $\vec{u}$ | velocity vector |
| $u$ | mean velocity component in the $x$-direction (m/s) |
| $u_{ij}$ | mean velocity normal to the grid surface ($\Delta x_i$, $\Delta y_j$) (m/s) |
| $U_i$ | mean velocity component in the $i$-direction (m/s) |
| $U_j$ | mean velocity component in the $j$-direction (m/s) |
| $v$ | mean velocity component in the $y$-direction (m/s) |
| $V_{i_{burn}}$ | volume of the $i$-th grid-cell in the burning room ($m^3$) |
| $V_P$ | grid-cell volume ($m^3$) |
| $W$ | Width of burning room doorway (m) |
| $w$ | mean velocity component in the $z$-direction (m/s) |
| $y^+$ | dimensionless distance from wall |
| $x$, $y$, z | Cartesian co-ordinates |

*Greek symbols*

| | |
|---|---|
| $\beta$ | thermal expansion coefficient (1/K) |
| $\Gamma_\varphi$ | diffusion coefficient in the conservation equations |
| $\Delta x_i$ | $x$-dimension of the opening grid-cell (m) |
| $\Delta y_j$ | $y$-dimension of the opening grid-cell (m) |
| $\varepsilon$ | turbulence dissipation rate ($m^2/s^3$) |
| $\varphi$ | time-average of instantaneous flow variable |
| $\varphi_P$ | value of flow variable at the central grid node, $P$ |
| $\varphi_I$ | value of flow variable at the neighbouring grid node, I |
| $\eta$ | expansion parameter |
| $\mu$ | dynamic laminar viscosity (kg/(ms)) |
| $\mu_t$ | dynamic turbulence viscosity (kg/(ms)) |
| $\rho$ | air density ($kg/m^3$) |
| $\rho_a$ | surrounding gas density ($kg/m^3$) |
| $\rho_{a1}$ | cold layer density ($kg/m^3$) |
| $\rho_{a2}$ | hot layer density ($kg/m^3$) |
| $\rho_r$ | burning-room air density ($kg/m^3$) |
| $\rho_\infty$ | ambient air density ($kg/m^3$) |
| $\sigma_h$ | turbulence Prandtl number for enthalpy |
| $\sigma_k$ | turbulence Prandtl number for kinetic energy of turbulence |
| $\sigma_\varepsilon$ | turbulence Prandtl number for dissipation rate of turbulence |

*Subscripts*

| | |
|---|---|
| $a$ | surrounding air |
| $B$ | buoyancy |
| Fuel | fuel |
| $g$ | gas |
| $I$ | neighbouring grid node |
| $i$, j | $i$, j directions |
| $i_{burn}$ | $i$-th cell within the burning room |
| $n_{burn}$ | number of cells within the burning room |
| $P$ | central grid node |
| $r$ | burning room |
| ref | reference |
| $t$ | turbulent |
| $\infty$ | ambient |

offer computational efficiency, as well as satisfactory accuracy for engineering purposes, especially in cases of simple geometries [10]. However, they supply limited information about the fire environment and, as the variables of interest are averaged over zones with large spatial scale, the resolution produced is poor and important local effects may be lost. Furthermore, a priori knowledge of the flow structure is needed, which can be found either by experimental measurements or from preliminary theoretical considerations. On the other hand, CFD models are based on the fundamental local conservation laws for physical quantities, such as mass, momentum, energy and chemical species concentrations, which form a set of partial differential equations. These equations are solved with the highest practically possible spatial and temporary resolution to yield distributions of the dependent flow variables, and thus they provide detailed information of the flow structure [1–3]. For this reason, CFD modelling is considered to be a more general and accurate method to deal with the problem of compartment fire. As the airflow is characterized by strong streamline curvature due to buoyancy forces, CFD modelling is considered as the most suitable tool for reliable airflow simulation. The more accurate the information for any re-circulation region, the more advanced the knowledge about local hazardous effects (hot gas layers and smoke plumes) in buildings; for example, the possibility of smoke confinement in certain regions of the indoor space. Since field models resort to the fundamental physical principles of the "flow mechanics", they may be decoupled from experimental studies, as long as they are comprehensively validated against prototype experimental cases, with relatively high confidence. The major drawback, contrary to zone models, is the computational cost, which may be prohibitive but which, however, gradually diminishes due to the continuous progress of computational technology.

One of the first field models for predicting flow induced by thermal sources is the MOSIE2 (Movement Of Smoke In Enclosures-

2D), presented by Markatos et al. [1]. In that work, that eventually evolved into the JASMINE (J Analysis of Smoke In Enclosures) code [11,12], the air velocity and temperature distributions were predicted in an enclosure containing a fire source. The problem was solved in a two-dimensional domain and the fire source was handled as a Volumetric Heat Source (VHS). The results appeared to be plausible and in good agreement with available experimental data. It was evident, however, that to validate thoroughly such a mathematical model either better experimental data with two-dimensional (2D) features should be obtained or that a three-dimensional (3D) version of the model should be employed for cases where more data is available. The above model was improved in Ref. [2], where the airflow movement was predicted in a 3D domain. The results were compared with available experimental data found in literature [13], and appeared relatively accurate. The method described revealed the usefulness and practicability of CFD for fire engineering applications.

Following the above pioneer studies, many investigations have been performed since, for the assessment of compartment fires, most common cases being those of one-room and two-room enclosures. A detailed experimental study referring to the first case was performed by Steckler et al. [13]. Experimental results concerning temperature and velocity distributions, as well as neutral-plane height and mass flow rates were obtained for various scenarios of heat source strengths and locations. These results served as data allocated for validation of various CFD models. For example, the CFD model described in Ref. [2] led to acceptable agreement with experimental results, using the VHS approach combined with the Standard $k$–$\varepsilon$ turbulence model, modified for buoyancy effects. Chow [14] also applied the modified Standard $k$–$\varepsilon$, coupled with the combustion process using the Simple Chemical Reaction System (SCRS) approach [15], according to which perfect combustion is assumed. However, apart from the combustion products distribution results, no significant improvement on temperature and velocity predictions was achieved. The performance of the modified Standard $k$–$\varepsilon$ model was further evaluated by Lewis et al. [16], who incorporated an eddy-break-up combustion model [17], with radiative heat transfer taken also into account. The predicted mass flow rates and neutral-plane height were in excellent agreement with the experimental data, although the performance of the simple VHS model [2] concerning these parameters was still unidentified. An attempt to calculate these critical factors may be found in [18], where different combustion models, e.g., the VHS, the Eddy-break-up model, and the presumed probability density function (prePDF), coupled with the modified Standard $k$–$\varepsilon$ model were used. It was found that all combustion models used failed to predict accurately the mass flow rate, the neutral-plane height, as well as the temperature and velocity variations. The simplest VHS model led to relatively better agreement with the experimental measurements, but still with large deviations [2]. Apart from the Standard $k$–$\varepsilon$ model, other models have also been tested, such as in Ref. [19]. The low-Reynolds-number $k$–$\varepsilon$ model, the standard $k$–$\varepsilon$ model, and a four-equation turbulence model were compared against experimental results and the inability of the second one to predict accurately the buoyancy production of turbulence kinetic energy was revealed. Applications of the modified Standard $k$–$\varepsilon$ to single-room fire may also be found in [20,21]. To the best of the authors' knowledge, no CFD simulations have been performed using a modified RNG $k$–$\varepsilon$ model [22], for single-room fires. A few studies which apply the RNG model for fire cases exist, but they refer only to cross flow effects on plume development [23] and to negligible turbulence kinetic energy buoyancy production [21].

In the second case of a two-room fire, various experimental studies exist to assess the airflow mechanism, and also to acknowledge the differences in comparison with one-room fires [24–26]. CFD modelling of the aforementioned experiments has also been performed, in order to extend CFD applications beyond the single compartment geometry. Such an extension was presented by Yeoh et al. [27] in the two-room compartment structure described in [25]. The combustion process, radiation modelling and turbulence, using the modified Standard $k$–$\varepsilon$ model, were taken into account. In agreement with previous single-room results [2,19–21], the VHS concept led to acceptable agreement with temperature and velocity measurements, but results deviated above the fire source. The flow through a doorway induced by a two-room compartment fire was investigated by Chow and Zou [28]. They used the Fire Dynamics Simulator (FDS), which applies Large Eddy Simulation (LES), to derive equations for calculating doorway flow rates induced by a fire corresponding to the experimental facility described in [24]. Numerical results obtained by CFD models concerning two- or (generally) multi-compartment fires may also be found in other investigations, as for example in [29]. For the case of two-room fires, as for singe room fires, no application of a modified RNG model, together with mass flow rates and neutral-plane heights calculations, was found.

Based on the literature review above, turbulence modelling of buoyancy-driven flows within buildings is still of major concern. The turbulence modelling can affect flow predictions by about the same amount as radiative heat fluxes [19], and the heat-release rate is the most important parameter for the accurate prediction of fire hazard [30]. The above considerations dictate the purpose of the present study. Turbulence effects were modelled using modified versions of the Standard $k$–$\varepsilon$ model and, for the first time to the authors' best knowledge, of the modified RNG $k$–$\varepsilon$ model for both single-room and two-room compartment geometries. The fire source is represented by a volumetric heat source. In the single-room case, comparisons between the numerical results obtained by both turbulence models and available experimental results, found in [13], are performed. In the two-room case, there are no experimental data for comparison, but the results obtained by the single-room-case validated model appear plausible. In both cases, important design factors, such as mass flow rates and neutral-plane heights are calculated, applying a special post-processing procedure, and the numerical results are validated with either available experimental data (single-room case) or results obtained by empirical correlations found in literature (two-room case).

## 2. Mathematical modelling

### 2.1. The physical problem

The physical problem considered is the movement of combustion products in 3D enclosures of a certain geometrical complexity. A typical compartment fire undergoes the following major stages [3,10]:

- Ignition: Pyrolysis of a fuel leading to gaseous volatiles releases, which are burnt as they mix with air.
- Growth: Hot gases are produced by the fire rise due to buoyancy entraining the surrounding air, and a fire plume is formed. Impingement of the fire plume on the ceiling gives rise to formation of a hot smoke layer in the upper part of the room, and the so-called hot upper layer begins to form. The upper layer volume still increases at a rate faster than the entrainment air into the fire, thus both upper layer gases and lower layer air leave the compartment.
- Flashover: Rapid transition from the growth period to a fully developed fire, resulting in the total surface of the combustible material being involved in fire.

- Fully developed fire: The heat-release rate reaches its maximum value, and the development of the fire is limited by oxygen availability. A quasi-steady situation prevails in which, cold external air flows into the compartment at the bottom of the vent and upper layer gases leave the room at the top of it.
- Decay: Heat-release rate diminishes as the fuel is consumed.

In the present study, the post-flashover fully developed fire stage is considered, as it represents the worst fire scenario. The expected flow field at this stage is illustrated in Fig. 1 for the cases of one- and two-room enclosures, with the fire source located in the left-hand room. The smoke and thermal distribution is represented by grey colour, while white colour represents external fresh air. Air suction through the opening occurs, caused by pressure differences due to buoyancy forces, associated with hot gas extraction through the upper part of the opening. This process leads to the formation of the so-called cold lower layer and the hot upper layer. Substantial design factors, such as the mass inflow and outflow rates, $\dot{m}_a$, $\dot{m}_g$, $\dot{m}_{g1}$, $\dot{m}_{g2}$, and also the neutral-plane heights of both the burning room ($N$) and the adjacent room ($H_h$) are illustrated in the sketches. In the problems considered, the flow is dominated by buoyancy and the turbulence serves to promote the rate of diffusion of heat, mass and momentum. Neither radiation nor combustion is included, the fire source being considered as a simple volumetric heat source (VHS approach). Non-uniform buoyancy forces are allowed to affect both the mean flow and the fluctuating motions.

### 2.2. The governing differential equations–assumptions

The independent variables of the steady-state problem are the three components ($x$, $y$, $z$) of a Cartesian coordinate system. The main dependent variables characterizing the flow are the three velocity components ($u$, $v$, $w$), pressure $p$, enthalpy $h$, kinetic energy of turbulence $k$ (Section 2.3), and the turbulence energy dissipation rate $\varepsilon$ (Section 2.3).

All these dependent variables, with the exception of pressure, appear as the subjects of equations of the general form [31,32]:

$$\frac{\partial(\rho\varphi)}{\partial t} + div(\rho\vec{u}\varphi - \Gamma_\varphi grad\varphi) = S_\varphi \tag{1}$$

where $\varphi$ is the dependent variable, e.g., velocity components, enthalpy, $k$ and $\varepsilon$, or 1 for the continuity equation, ρ the Fluid density, $\vec{u}$ the Velocity vector, $\Gamma\varphi$ the "effective" exchange coefficient of $\varphi$ and $S_\varphi$ is Source rate per unit volume.

The flow was assumed to take place under steady-state conditions, thus the general conservation Eq. 1 for all dependent variables is implemented, for steady-state simulations:

$$div(\rho\vec{u}\varphi - \Gamma_\varphi grad\varphi) = S_\varphi \tag{2}$$

The pressure variable is associated with the continuity equation

$$div(\rho\vec{u}) = 0 \tag{3}$$

in anticipation of the so-called pressure–correction equation [33], which is deduced from the finite-domain form of Eq. 3. Further details may be found, for example, in [1,2]. The momentum and enthalpy conservation equations are implemented for steady-state simulations (Eq. 2) and are as follows:

$$\rho U_j \frac{\partial U_i}{\partial x_j} = -\frac{\partial P}{\partial x_i} + \frac{\partial}{\partial x_j}\left[(\mu+\mu_t)\left(\frac{\partial U_i}{\partial x_j}+\frac{\partial U_j}{\partial x_i}\right)\right] + \rho g_i \beta(T - T_{ref}) \tag{4}$$

$$\rho U_j \frac{\partial h}{\partial x_j} = \frac{\partial}{\partial x_j}\left\{\left(\frac{\mu}{P_r}+\frac{\mu_t}{\sigma_T}\right)\frac{\partial h}{\partial x_j}\right\} + \rho S_h \tag{5}$$

### 2.3. Turbulence models applied

Two turbulence models were used in the present study, together with the Boussinesq approximation for buoyancy effects: (a) The standard $k$–$\varepsilon$ model [34], (b) The RNG $k$–$\varepsilon$ model [35]. The models use the logarithmic "wall-functions" near solid surfaces ($11.5 < y^+ < 150$) [34]. The validity of Boussinesq's approximation was tested here by repeating runs using variable density (as a perfect-gas-law function of temperature), and was found adequate.

#### 2.3.1. Standard k–ε model

This model solves for the kinetic energy of turbulence $k$, and the energy dissipation rate $\varepsilon$. The model is modified to account for buoyancy effects on turbulence [1,2]. The governing equations, cast in the form of Eq. 2, are presented below:

- Kinetic energy of turbulence, $k$.

$$\rho u_j \frac{\partial k}{\partial x_j} = \frac{\partial}{\partial x_j}\left[\left(\mu+\frac{\mu_t}{\sigma_k}\right)\frac{\partial k}{\partial x_j}\right] + P_k + G_B - \rho\varepsilon \tag{6}$$

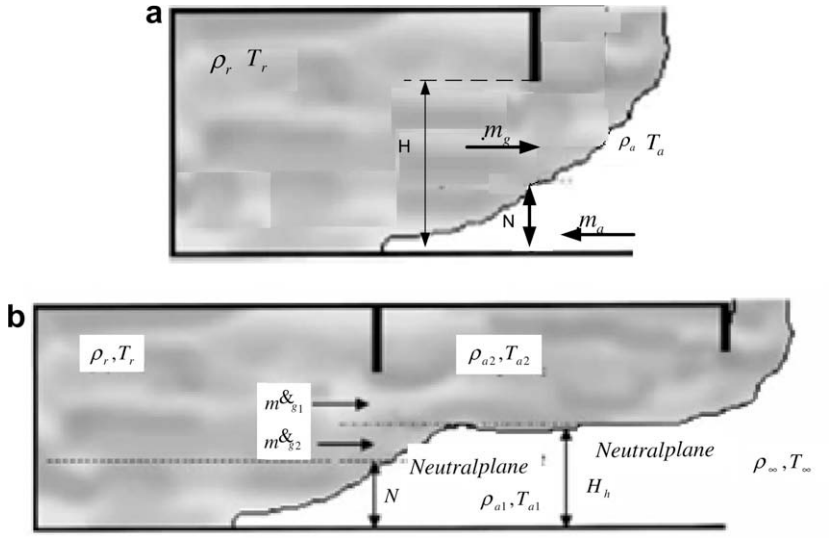


**Fig. 1.** Fully developed fire in: (a) one-room compartment; and (b) two-room compartment.

- Energy dissipation rate, $\varepsilon$.

$$\rho u_j \frac{\partial \varepsilon}{\partial x_j} = \frac{\partial}{\partial x_j}\left[\left(\mu + \frac{\mu_t}{\sigma_\varepsilon}\right)\frac{\partial \varepsilon}{\partial x_j}\right] + \frac{\varepsilon}{k}(C_1 P_k - C_2 \rho \varepsilon + C_3 G_B) \quad (7)$$

- Turbulence viscosity. In the above model, turbulence viscosity is computed by:

$$\mu_t = \rho C_\mu \frac{k^2}{\varepsilon} \quad (8)$$

- Empirical constants. There are six empirical constants involved, as follows:

$$C_1 = 1.44, \quad C_2 = 1.92, \quad C_3 = 1.0, \quad C_\mu = 0.09, \quad \sigma_k = 1.0, \quad \sigma_\varepsilon = 1.3 \quad (9)$$

*2.3.2. RNG k–ε model*

The RNG (Renormalization Group) model by Yakhot and Orszag [35] accounts for effects of small-scale turbulence using a random function in the Navier–Stokes equations. The RNG process removes the small-scale motions from the equations by expressing their effects in terms of larger-scale motions and a modified viscosity. In the present work, this model is modified to account for buoyancy effects on turbulence. The governing equations of the modified model are as follows:

- Kinetic energy of turbulence, $k$.

$$\rho u_j \frac{\partial k}{\partial x_j} = \frac{\partial}{\partial x_j}\left[\left(\mu + \frac{\mu_t}{\sigma_k}\right)\frac{\partial k}{\partial x_j}\right] + P_k + G_B - \rho \varepsilon \quad (10)$$

- Energy dissipation rate, $\varepsilon$.

$$\rho u_j \frac{\partial \varepsilon}{\partial x_j} = \frac{\partial}{\partial x_j}\left[\left(\mu + \frac{\mu_t}{\sigma_\varepsilon}\right)\frac{\partial \varepsilon}{\partial x_j}\right] + \frac{\varepsilon}{k}(C_1 P_k - C_2 \rho \varepsilon + C_3 G_B) - R \quad (11)$$

- Turbulence viscosity. In the RNG model, turbulence viscosity is computed by:

$$\mu_t = \rho C_\mu \frac{k^2}{\varepsilon} \quad (12)$$

- Empirical constants. There are also six empirical constants for the RNG model:

$$C_1 = 1.42, \quad C_2 = 1.68, \quad C_3 = \tanh|u/v|, \quad C_\mu = 0.0845, \quad \sigma_k = 0.719, \quad \sigma_\varepsilon = 0.719 \quad (13)$$

In both models, $P_k$ represents the generation of turbulence kinetic energy due to the mean velocity gradient, and is defined by $P_k = \mu_t\left(\frac{\partial U_i}{\partial x_j} + \frac{\partial U_j}{\partial x_i}\right)\frac{\partial U_i}{\partial x_j}$.

The difference between the standard and RNG $k$–$\varepsilon$ models is actually, apart from the different constants, the presence of an additional strain-rate term R in the ε-equation for the latter (Eq. 11). The term is modelled as $R = \frac{C_\mu \eta^3 (1-\eta/\eta_0)}{1+\beta_1 \eta^3}\frac{\varepsilon^2}{k}$, where $\eta = Sk/\varepsilon$ and $S = (S_{ij}S_{ij})^{1/2}$. The term $S_{ij} = \frac{1}{2}\left(\frac{\partial U_i}{\partial x_j} + \frac{\partial U_j}{\partial x_i}\right)$ is the mean rate of strain and $U$ the velocity of the mean flow. The significance of the inclusion of this term is its responsiveness towards the effects of rapid rate strain and streamlines curvature, which cannot be properly represented by the standard $k$–$\varepsilon$ model.

In the models described above the quantity $G_B$ is included (Eqs. 6, 7, 10, and 11), to represent the production/dissipation of turbulence energy due to the action of buoyancy forces [1,22], computed by:

$$G_B = -\beta g \frac{\mu_t}{\sigma_{t,\varphi}}\frac{\partial T}{\partial y} \quad (14)$$

where $\beta = 1/T_{ref}$ is the thermal expansion coefficient. It is expected, and it is supported by other investigations, that different temperature predictions will be obtained by the aforementioned turbulence models. For example, it has been proven that different temperature variations are produced in case of cavity flows, and this difference increases as the aspect ratio increases [22]. This is not surprising due to the presence of the term $G_B$ in Eqs. 6, 7, 10, and 11, that expresses the buoyancy production/destruction of turbulence kinetic energy. Turbulence kinetic energy values calculated by Eqs. 6 and 10 differ due to different empirical coefficients and, more importantly, due to different values of the calculated dissipation rate, which participates in the turbulence kinetic energy calculations, by Eqs. 7 and 11. Differences in the buoyancy production of turbulence kinetic energy causes differences in temperature gradients predicted by the different turbulence models applied, leading to different outcomes of the energy Eq. 5. The same situation is true even if the term $G_B$ is neglected in the Eqs. 7 and 11, as long as it remains in Eqs. 6 and 10 [1,2,36]. A more complicated model, such as the RNG, is not necessarily better suited to problems with strong heat fluxes but it is, theoretically at least, better suited to flows with rapid rate-of-strain and with streamline curvature; and strong heat fluxes may lead to the latter effect. In general, this is a case-sensitive matter and any a priori statement of the turbulence model performance would be inappropriate. For this reason both turbulence models are tested in the present study, as this task is one of its purposes.

## 3. Method of solution

### 3.1. Formulation of equations

The space (and time when necessary) dimensions are discretized into finite intervals and the variables are correspondingly computed at only a finite number of locations in three-(or four-) dimensional space, i.e., at the so-called "grid points". These variables are connected with each other by algebraic equations, derived from their differential counterparts by integration over the control volumes defined by the above-mentioned intervals [31].

### 3.2. Solution procedure

The procedure adopted for the solution of the algebraic equations, derived as in Section 3.1 above, is the SIMPLEST algorithm [2,36]. The difference of this procedure from the well established SIMPLE [33] is that the finite-domain coefficients of the momentum equations contain only diffusion contributions, the convection terms being added to the linearized source term of the equations [37]. This practice was found to eliminate the need for severe under-relaxation of the pressure-correction, particularly for very fine grids, thus accelerating convergence.

### 3.3. Boundary conditions

For the problems considered there are two types of boundaries: solid or free. On a solid boundary, the no-slip condition for the velocity components is employed. For the temperature equation, adiabatic sidewalls, floor and ceiling are applied, while the fire source is modelled as a volumetric heat source. The fluxes of

momentum and heat to the wall obey the wall-function relations of Launder and Spalding [38]. For the kinetic energy of turbulence, the zero diffusive flux at the wall is used. For the dissipation rate, the empirical evidence that a typical length scale of turbulence varies linearly with the distance from the wall, is used to calculate $\varepsilon$ itself at the near-wall point. Finally, at the free boundaries the pressure is prescribed as follows: A fixed pressure (atmospheric pressure) is assumed to prevail outside the free boundary; the mass inflows and outflows being an outcome of the solution procedure. Velocities and temperatures at the free surfaces outside the enclosure are taken equal to the ambient conditions.

### 3.4. Initial conditions

The simulations reported here refer only to the steady state. Therefore, computations start using either guesses or the solutions of a previous similar run as initial conditions.

### 3.5. Computational details

The finite-volume method [31] was used to solve the set of conservation equations. The domain of interest was divided into a number of control volumes. Over a control volume about the point $P$, the set of differential equations for $\varphi$ is integrated to give discretized algebraic equations of the form [1]:

$$a_P\varphi_P = \sum_I a_I\varphi_I + S_{\varphi,P}V_P \tag{15}$$

where $a_I$ represents coefficients, $I$ stands for the neighbouring nodes around the central one, $P$, $S_{\varphi,P}$ is the source term of the transferred variable $\varphi$, and $V_P$ is the grid-cell volume. In solving the discretized Eq. 15, the sum of absolute normalised residuals *RES* over a control volume about the central node $P$ is defined as:

$$RES = \sum_{all\ grid\ cells} \left| \sum_I a_I\varphi_I + S_{\varphi,P}V_P - a_P\varphi_P \right| \tag{16}$$

Steady-state computations were stopped when $RES = 10^{-3}$, and convergence is considered to be obtained when the total residual error in the field is less than 0.1% of the reference values for each variable, which are the mass flow rate, the inlet momentum flux and the inlet energy flux. To ensure convergence, relaxation of the "false-time-step" was employed for all variables except pressure for which linear relaxation was used [37].

The CPU time required for the optimum grids for the problems considered to obtain full convergence of solution was about 240 min and 360 min for the one-room (63,240 cells, see Section 4.2) and two-room enclosures (105,400 cells, see Section 4.3), respectively, on a Linux PC (Pentium IV, 2.4 GHz CPU and 1 GB of RAM).

### 3.6. Mass flow rate calculations

The airflow rate into or out of a building can be calculated by integrating the normal velocity at the opening of a building, when the flow is incompressible, which is true for most naturally ventilated compartment fires. Based on the mass balance of the airflow within the enclosure (see Fig. 1), the mass outflow rate equals to the sum of the fuel burning rate and the mass inflow rate through the opening, as follows [28,39,40]:

$$\dot{m}_g = \dot{m}_{fuel} + \dot{m}_a \tag{17}$$

In the present study, because combustion was simulated by the VHS concept, there will be as much fluid leaving the building, as there will be fluid entering the building, i.e., $\dot{m}_g = \dot{m}_a$. The mass ouflow rate is selected for macroscopic quantification of the flow field for both cases studied, since it represents an additional indicator of thermal plume development. Utilizing the CFD results, the mass outflow rate through the doorway of the burning room may be calculated by integrating the velocity at the outflow region (above neutral-plane height) of the vent. This can be achieved numerically by the summation of the velocity stored in each grid-cell in $x$ and $y$ directions, as follows:

$$\dot{m}_g = \rho_r \sum_{j=1}^{m}\sum_{i=1}^{n} u_{ij}\Delta x_i \Delta y_j \tag{18}$$

where $\rho_r$ is the air density of the hot upper layer leaving the room, $u_{ij}$ is the velocity stored in the i-th and in the j-th cell along x and y directions (where $\sum_{i=1}^{n}\Delta x_i = width\ of\ opening$, and $\sum_{j=1}^{m}\Delta y_j = above\ neutral-plane\ height\ of\ opening$), respectively, corresponding to the grid-cell surface $\Delta x_i \cdot \Delta y_j$ at the opening, and, finally, $m$ and $n$ are the number of the outflow grid cells at the $y$ (above neutral plane) and $x$ directions, respectively.

## 4. Results and validation

### 4.1. General description of the cases considered

Two different compartment geometries have been examined for demonstration and validation purposes. The first is an enclosure comprising one room, a door that plays the role of both an inlet and an outlet and a heat source at the centre of the room. For this problem experimental data are available for different heat sources and different locations of the source in the room. Further details of the experimental setup may be found in [13]. In the present paper, results for a heat source of 62.9 kW at the centre of the room are presented and discussed, in the form of air temperature distribution and velocity vectors. Following satisfactory agreement of the results with experiments, a two-room structure with a fire source in one of them is simulated. The two rooms are of the same dimensions with the room of the previous single-room problem. The fire source is considered to be again a heat source of 62.9 kW located at the centre of the first room. The door between the two rooms and the outside door have the same dimensions with the door of the single-room problem.

### 4.2. Single-room enclosure

The fire experiments of Steckler et al. [13] were performed in a rectangular compartment, of side 2.8 m and height 2.18 m, incorporating ceramic fiber board insulation and a circular gas burner of diameter 0.3 m, fuelled by commercial-grade methane. The layout of that room is illustrated in Fig. 2(a). Of the several variations in burner position and ventilation configuration reported in [13], the present paper illustrates the results obtained when the burner is positioned centrally in the room and ventilation is provided by a room opening (doorway) of 1.83 m height and 0.74 m width. The rest of the results obtained are similar with respect to the experimental measurements, as those for the reported case. The fuel flow rate selected corresponds to a heat output of 62.9 kW. Conditions at the opening attracted particular attention and detailed measurements of temperature, using aspirated thermocouples, and of velocity by bi-directional probes were reported. The measuring devices were positioned at the centreline of the doorway and at the point "corner" of the room located at a distance of 0.305 m from the right-hand wall and 0.305 m from the west wall.

The assumptions of the CFD simulation were:

- one-phase, steady-state flow of a Newtonian fluid;
- adiabatic walls (since the walls and ceiling were covered with a ceramic fiber insulation board); and,

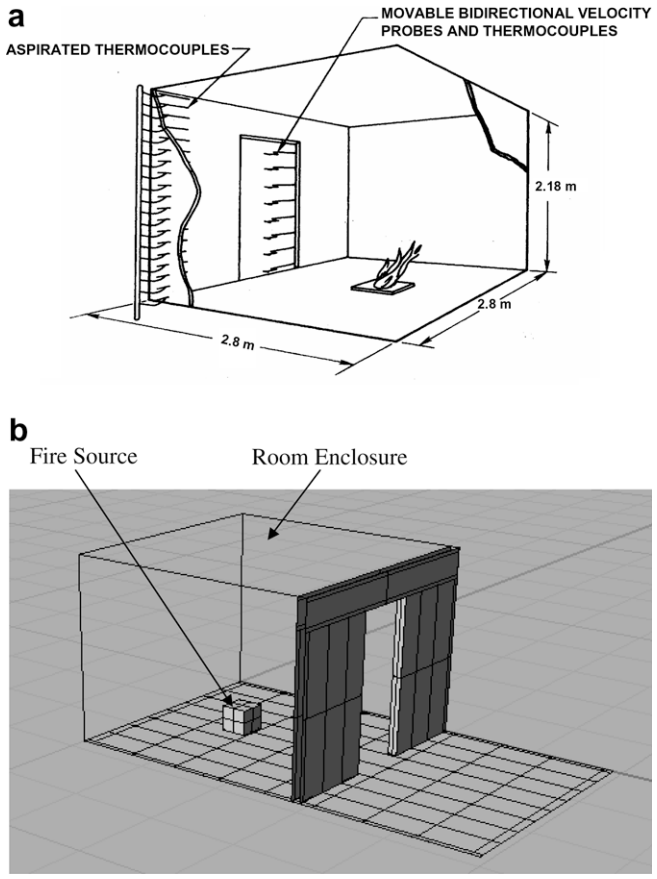


**Fig. 2.** (a) Schematic of compartment fire; (b) model geometry.

- the fire source is modelled as a volumetric heat source of 0.3 m × 0.3 m × 0.3 m, while radiation is neglected. The volumetric heat capacity of 62,900 W/(0.027 $m^3$) is used as an input parameter that is fed into the source term of the energy Eq. 5, as follows: $\dot{q}''' = 2.329 \cdot 10^6 J/(m^3 s) = \rho S_h$.

The geometry considered is shown in Fig. 2(b). Several grid sizes were employed to test sensitivity of the solutions to grid refinement. The solution that proves to be virtually independent of further grid refinement is that obtained by using a grid of 40 × 31 × 51 ($x$–$y$–$z$ axis, respectively). Fig. 2(b) presents the computational domain that was extended 2.18 m outside the room to simulate the entrainment of fresh air through the doorway correctly [2,38]. The coordinate system has its origin at the left-hand corner of the room floor, with the $z$-axis directed along the enclosure.

Fig. 3 presents numerical results, obtained using the Standard $k$–$\varepsilon$ model, of temperature and velocity variations at the middle longitudinal plane of the solution domain. The airflow motion is clearly dominated by buoyancy forces produced around the burner at the middle of the enclosure, and it may be described as follows: As air passes across the heat source, its temperature increases, thus its density decreases. Because of the buoyancy forces that arise due to density variations, the hot air rises towards the top space of the enclosure. When the hot layer reaches the right vertical wall it descends and exits through the top of the doorway, while fresh air enters the room through the bottom. The displacement of indoor air by the entering external air, due to air suction caused by indoor–outdoor pressure differences, leads to a re-circulation region at the middle of the room which maintains the expected hot upper and cold lower layer, as already sketched in Fig. 1(a) of the estimated flow field.

The next step is to examine the performance of the buoyancy-modified turbulence models used. Comparisons among the results of the modified $k$–$\varepsilon$ model, the modified RNG $k$–$\varepsilon$, and the experimental data are presented, at the physical locations where data are available, i.e., the measurement sites depicted in Fig. 2(a). In Fig. 4(a), the air velocity at the doorway centreline is presented. Comparisons among the two models and the experimental results are shown. In Fig. 4(b) the temperature distribution at the doorway centreline is shown and the same comparisons have been made. In Fig. 4(c), the temperature distribution at the "corner" of the room is presented.

The numerical results for velocity are generally in fair agreement with the experimental data, using both turbulence models. More specifically, the divergence, in terms of mean absolute error, of the computed velocity from the measured one at the outflow region above neutral-plane height (1.028 m, Fig. 4(a)), is estimated at 10% and 15% using the Standard $k$–$\varepsilon$ and the RNG $k$–$\varepsilon$ model, respectively. The corresponding divergence across the inflow region is 35% and 30% for the two models. It is seen that both models over-predict the inflow velocity, while they perform relatively better above the neutral-plane height. Generally, both turbulence models provide equivalent predictions of the bi-directional flow through the vent. As far as the doorway temperature variations are concerned, inspection of Fig. 4(b) reveals that the RNG model provides more accurate predictions at the hot upper layer region, while at the cold lower layer both models produce similar results. Particularly, the Standard $k$–$\varepsilon$ model discrepancy to measurements is about 6%, reducing to 3% when the RNG model is used. The same observation is true at the "corner" of the enclosure (Fig. 4(c)), where the RNG model leads to a 7% difference compared to the experimental recordings, and the Standard $k$–$\varepsilon$ model results deviate by about 12%. It is concluded that results by both models are in rather satisfactory agreement with temperature measurements within the hot upper layer, with the RNG $k$–$\varepsilon$ model leading to relatively more accurate computations. The numerical errors in the cold lower layer temperature predictions are higher, by around 10%, for both models, within the region below the neutral-plane height through the doorway (Fig. 4(b)). Even more, the RNG model produces a large error of 32% at the "corner's" lower region. However, qualitatively the predicted temperature gradient is similar to the experimental one, and thus the temperature distribution obtained by the RNG $k$–$\varepsilon$ model is similar to that of the measurements (see Fig. 4(c)). The discrepancies between predicted and measured temperatures may be attributed either to the omission of radiant heat transfer from the upper hot layer to the lower cold layer in the present models, or to measurement errors due to possible higher temperature recordings than that of the surrounding gas, due to the fact that the thermocouples pick up radiation from the flames and the heated walls [10]. In general, however, the VHS model applied in this study is considered satisfying, at least for practical engineering purposes, using either of the turbulence models, while the temperature of the hot upper layer is better predicted using the modified RNG $k$–$\varepsilon$ model. The predicted flow field proves the effectiveness of the CFD model used and its usefulness in computing thermal plume development.

As discussed in Section 1, other macroscopic factors, such as the neutral-plane height and mass flow rates are critical design parameters in compartment-fire studies, as the opening plays the role of escape, or fire-fighting, passage. Results for these two design parameters, obtained using both the present CFD model and available empirical correlations [13], for the single-room compartment, are tabulated in Table 1. The measured height of the boundary between hot and cold layers is 1.028 m [13], while the predicted one is 1.053 m using the Standard $k$–$\varepsilon$ model, and 1.042 using the RNG

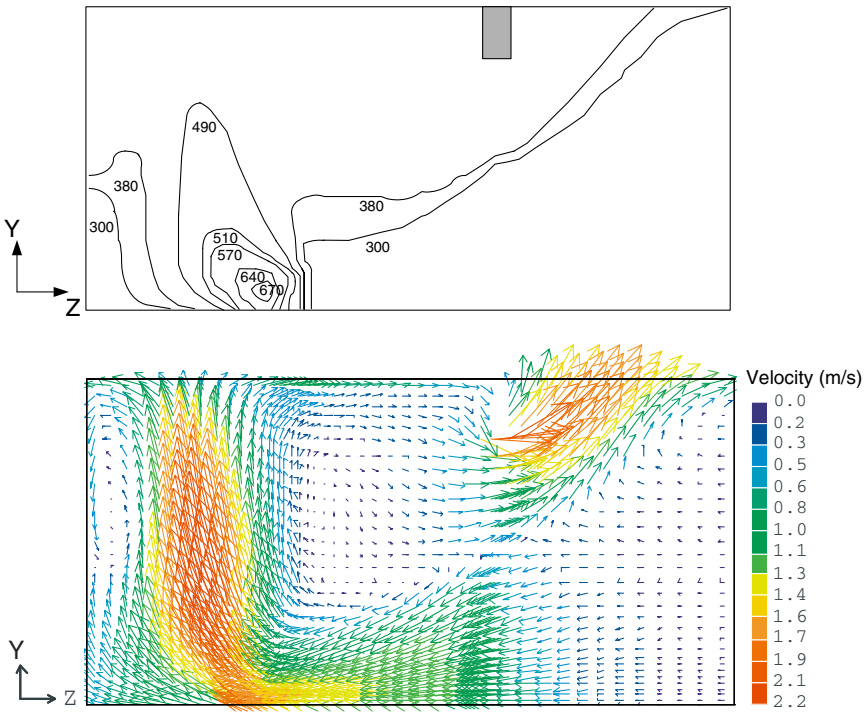


**Fig. 3.** (a) Temperature contours (K); and (b) Velocity vectors at the $y$–$z$ plane at position $x$ = 1.4 m.

$k$–$\varepsilon$ model, i.e., a difference of only about 2.5% and 1%, respectively. In the present study, neutral-plane heights are estimated following a regression technique utilizing the numerical results, through the doorway centreline, to yield a polynomial function of height; the height of minimum velocity is then calculated following an iterative procedure (Newton–Raphson). As far as the mass outflow rate is concerned, CFD velocity results are incorporated in Eq. 18 to yield an error of only about 0.35% and 5%, in comparison with the experimental value, using the Standard $k$–$\varepsilon$ and the RNG $k$–$\varepsilon$ model, respectively. It is observed that the deviation obtained using the RNG model is higher, although acceptable, in comparison with previous studies using combustion models [16]. In order to have an overall overview of the usefulness of the CFD model, empirical correlations of $\dot{m}_g$, such as Eq. 19 below [13], are also applied using, for comparison purposes, information by both the CFD results and the experimental measurements:

$$\dot{m}_g = \frac{2}{3}\sqrt{2g}C_0\rho_a A H^{1/2}\left[\frac{T_a}{T_r}\left(1-\frac{T_a}{T_r}\right)\right]^{1/2}\left(1-\frac{N}{H}\right)^{3/2} \tag{19}$$

Thus, in Eq. 19 $T_r$ is either found from experiments or it is calculated as follows:

$$T_r = \begin{cases} \textit{Either from experimental results} \\ \textit{OR} \\ \dfrac{\sum_{i_{burn}=1}^{n_{burn}} T_{i_{burn}} V_{i_{burn}}}{\sum_{i_{burn}=1}^{n_{burn}} V_{i_{burn}}} (i_{burn} = \textit{Burn-room cell of } V_{i_{burn}} \textit{ volume}), \\ \textit{for the CFD results} \end{cases} \tag{20}$$

and N is the neutral-plane height either found [13], or predicted by the CFD runs; in the latter case, it is calculated as discussed earlier. As presented in Table 1, the outflow rate is improved using the RNG model, in comparison with the corresponding value calculated using experimental information by Eq. 19. The error is only about 1.5%, and even better (error: 1.2%) compared to the measured outflow rate. Correspondingly, the Standard $k$–$\varepsilon$ leads to higher deviations of about 4% and 1.5%. This is not surprising as in Eq. 19 no-velocity information is used, and thus, since the RNG model leads to better temperature predictions in the hot upper layer, it provides a mass flow rate closer to the one calculated by Eq. 19, using experimental information, as well as to the measured one found in [13]. Comparing the numerical mass outflow rate (Eq. 18) with results obtained by Eq. 19 when utilizing CFD data, it is seen that they converge to a similar solution and thus both calculation methods (velocity utilization-CFD method, and no-velocity utilization-Empirical method) provide valid results.

Since the maximum changes of the dependent variables of the problem occur near the heat source, it is important to present the velocity and temperature distributions at the $y$–$x$ plane at the heat source. In Fig. 5 these distributions, as predicted by the RNG $k$–$\varepsilon$ model, are illustrated. The graphs show the structure of the simulated flow field above the source, with the air vortices creating the expected cold and hot layers. Fig. 6 shows the variations of velocity and temperature at the source centreline. Although no experimental data exist in this region, the information provided may serve for future comparisons among several combustion and radiation models to investigate the validity of the simple VHS model within the region close to the source.

Conclusively, the CFD model described, applying the simple VHS concept is considered fairly satisfactory for flow field and other design factors predictions. Both turbulence models applied provide reliable information about the airflow structure and the fire endurance [30] of the enclosure, as shown by comparisons with measurements and empirical correlations. As far as results in the hot upper layer are concerned, the RNG model predicts the thermal stratification and the neutral-plane height more accurately.

### 4.3. Two-room enclosure

The problem is extended to a two-room geometry, as shown in Fig. 7. The rooms communicate via a door and the right-hand room has its own doorway that plays the role of the air inlet–outlet. The

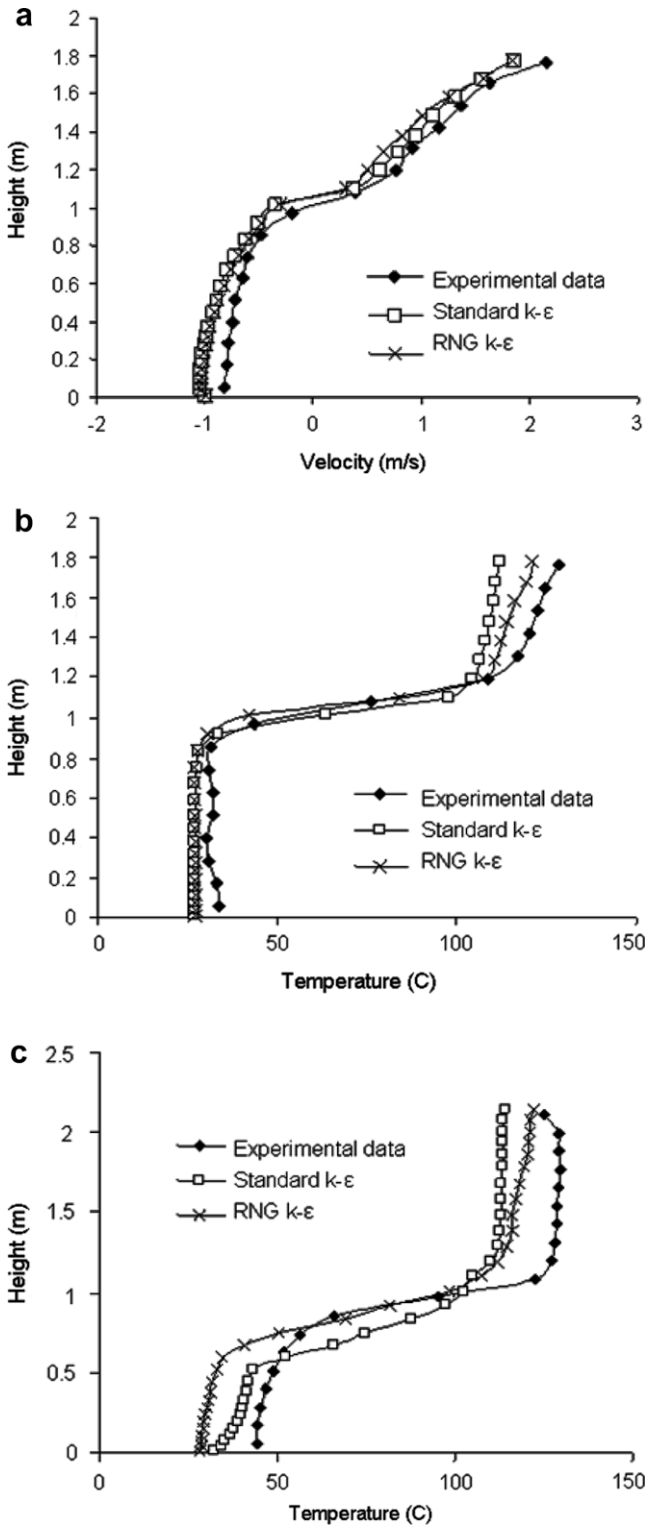


**Fig. 4.** Doorway centreline: (a) velocities; (b) temperatures, located at ($x$ = 1.4 m, $z$ = 2.851 m); and (c) Corner stack temperatures, located at ($x$ = 0.305 m, $z$ = 2.495 m).

rooms are of the same dimensions as in the previous problem, and so are the doors. The heat source is positioned at the centre of the left-hand room and is of a heat output of 62.9 kW. The left-hand room that contains the fire source is named "Burning room" and the right-hand one is named "Adjacent room".

A typical two-room compartment fire and its characteristic flow properties are presented in Fig. 1(b). In this figure, the fire spreading mechanism is presented in terms of mass flow rate [28]. The mass outflow rate through the doorway of the burning room is a result of the contribution of the neutral-plane heights of the two rooms ($N$ and $H_h$). Thus, the total mass outflow rate is defined as $\dot{m}_g = \dot{m}_{g1} + \dot{m}_{g2}$. Since the generation of these mass flow rates is created by the outflow velocity at the burning-room doorway, it is important to quantify the flow at this region. In the present study, this quantification at the doorways, as well as the calculation of the characteristic flow properties, are provided by the simulation of the flow throughout the compartment for evaluating fire spreading, particularly through these openings that are actually escape passages in case of fire.

The assumptions are the same as in the problem described in Section 4.2. A grid-independent solution is obtained using a grid of $40 \times 31 \times 85$. The computational domain was again extended outside the room to simulate entrainment of fresh air through the doorway. The coordinate system has its origin at the left-hand corner of the burning-room floor, with the $z$-axis directed along the enclosure. The problem is solved using again both the modified Standard $k$–$\varepsilon$ model and the modified RNG $k$–$\varepsilon$ model, and calculations of important design parameters, e.g., mass flow rates and neutral-plane heights, are performed. Since no experimental data exist to compare the CFD results with, validations are based on comparisons of mass outflow rates obtained by the CFD method (Eq. 18) and those obtained by available empirical correlations for two-room fires [28]. Finally, comparisons of temperature and velocity, as predicted by the turbulence models, at the doorway centreline of the burning room and the doorway centreline of the adjacent room are also presented.

One of the first empirical formulations to quantify the mass outflow rate is that provided by Nakaya et al. [24], who performed measurements in a prototype two-room enclosure containing a propane burner. Burning-room doorway velocity and temperature recordings were obtained and the mass flow rates were calculated using measured velocities through the opening. Based on Bernoulli's equation and on the assumption that in the burning room an upper layer of uniform temperature prevails, the mass outflow rate is calculated as follows [24]:

$$\dot{m}_g = C_0 W \rho_\infty T_\infty \sqrt{\frac{2g}{T_r}} \left\{ \left( \frac{1}{T_{a1}} - \frac{1}{T_r} \right)^{1/2} (H_h - N)^{3/2} + \frac{2}{3} \left( \frac{1}{T_{a2}} - \frac{1}{T_r} \right)^{-1} \cdot \left[ \left[ \left( \frac{1}{T_{a1}} - \frac{1}{T_r} \right)(H_h - N) + \left( \frac{1}{T_{a2}} - \frac{1}{T_r} \right)(H - H_h) \right]^{3/2} - \left[ \left( \frac{1}{T_{a1}} - \frac{1}{T_r} \right)(H_h - N) \right]^{3/2} \right] \right\} \quad (21)$$

Chow and Zou [28] acknowledged the non-uniformity of temperature in the hot upper layer of the burning room and proposed a simpler formulation of Eq. 21, as follows:

$$\dot{m}_g = \dot{m}_{g1} + \dot{m}_{g2} = \frac{2}{3} C_d \rho_\infty T_\infty \sqrt{2g} W H^{3/2} \cdot \sqrt{\frac{1}{T_r} \left( \frac{1}{T_{a1}} - \frac{1}{T_r} \right) \left( \frac{H_h - N}{H} \right)} \left[ \left( \frac{H_h - N}{H} \right) + \frac{3}{2} \left( 1 - \frac{H_h}{H} \right) \right] \quad (22)$$

where $T_r$ is the burning-room temperature, computed using Eq. 20.

In the present investigation, the performance of the turbulence models was tested using both the empirical Eqs. 21 and 22, formulated for the calculation of the outflow rates in two-room structures containing a fire source in the first room. Both Equations were used with CFD results, as no experimental data exist. Results

**Table 1**
Mass flow rates and neutral-plane heights for both cases considered.

| Flow parameters | N (m) | $H_h$ (m) | $\dot{m}_g$ (kg/s) Eq. 18 | $\dot{m}_g$ (kg/s) Eq. 19 | $\dot{m}_g$ (kg/s) Eq. 21 | $\dot{m}_g$ (kg/s) Eq. 22 | $\dot{m}_g$ (kg/s) measured | $\dot{m}_a$ (kg/s) measured |
|---|---|---|---|---|---|---|---|---|
| *One-room enclosure* | | | | | | | | |
| Experiment | 1.028 | – | – | 0.587 | – | – | 0.571 | 0.554 |
| Standard $k$–$\varepsilon$ | 1.053 | – | 0.569 | 0.563 | – | – | | |
| RNG $k$–$\varepsilon$ | 1.042 | – | 0.540 | 0.578 | – | – | | |
| Lewis et al. [16] | 0.999 | – | 0.523 | – | – | – | | |
| *Two-room enclosure* | | | | | | | | |
| Experiment | – | – | – | – | – | – | – | – |
| Standard $k$–$\varepsilon$ | 0.887 | 1.146 | 0.587 | – | 0.595 | 0.513 | – | – |
| RNG $k$–$\varepsilon$ | 0.887 | 1.131 | 0.536 | – | 0.572 | 0.521 | – | – |

The symbol "–" means not available value.

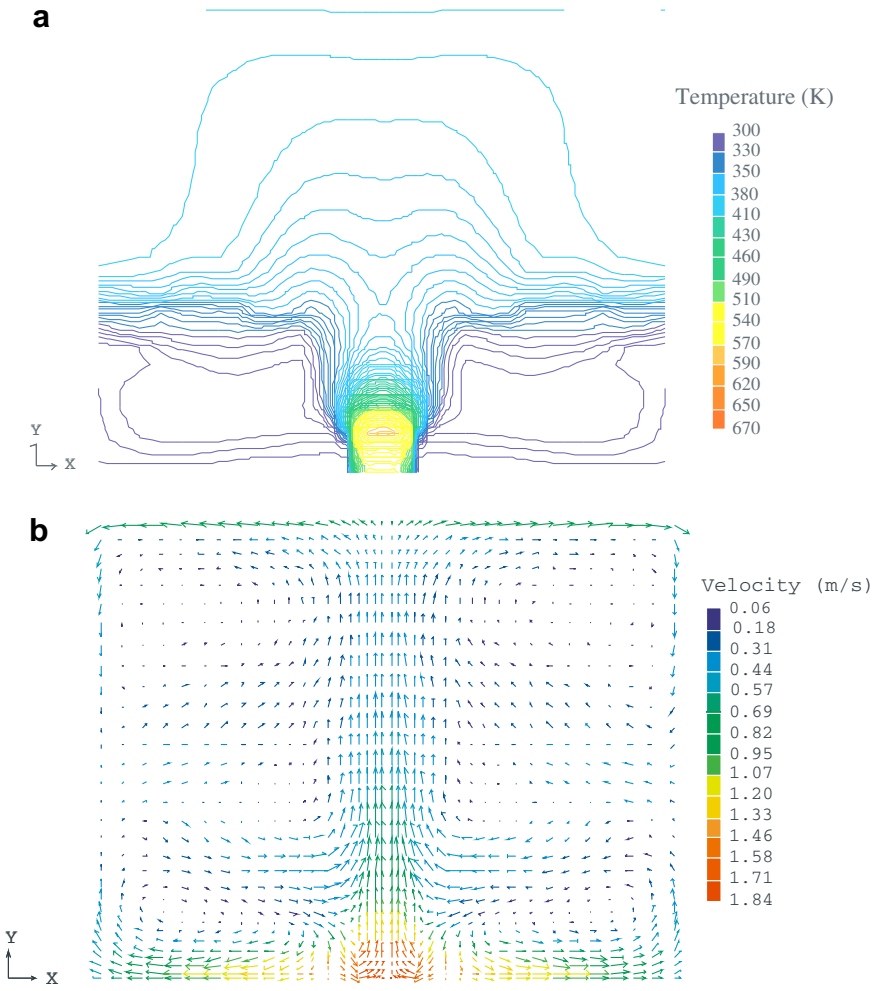


**Fig. 5.** (a) Temperature contours; (b) velocity vectors, at the plane $y$–$x$ at the position $z$ = 1.4 m.

obtained by the CFD solution (using Eq. 18) through the opening of the burning room, and by the empirical correlations above, are summarized in Table 1, together with the outflow rates of the first case (single-room enclosure). No substantial difference of mass outflow rate through the burning-room vent, between the single-room and the two-room compartments is observed. Referring to the neutral-plane height through the burning-room doorway, it is found that both models result to the same value (see Table 1), while a small difference exists for the neutral-plane height in the adjacent room. The calculation procedure of both neutral-plane heights is the same as that described in Section 4.2. In the adjacent room, $H_h$ is calculated using temperature results in the middle of the adjacent room, and only a difference of 1.3% between the Standard $k$–$\varepsilon$ and the RNG $k$–$\varepsilon$ model is observed. Referring to the mass flow rates obtained by Eq. 18, the difference between the turbulence models is 9.5%. The corresponding discrepancy of Eq. 21 to predictions by the Standard $k$–$\varepsilon$ and the RNG $k$–$\varepsilon$ model is 1.3% and 6.5%, respectively. It is seen that, as in the case of the single room, the RNG $k$–$\varepsilon$ model differs more than the Standard one from the empirical value. However, this is not true when Eq. 22 is used instead of Eq. 21. Then, the difference of the mass flow rate produced by the Standard $k$–$\varepsilon$ (Eq. 18) from the empirical one is greater than that obtained by the RNG $k$–$\varepsilon$ model. This may be due to the fact that the RNG predicts higher and more accurate tempera-

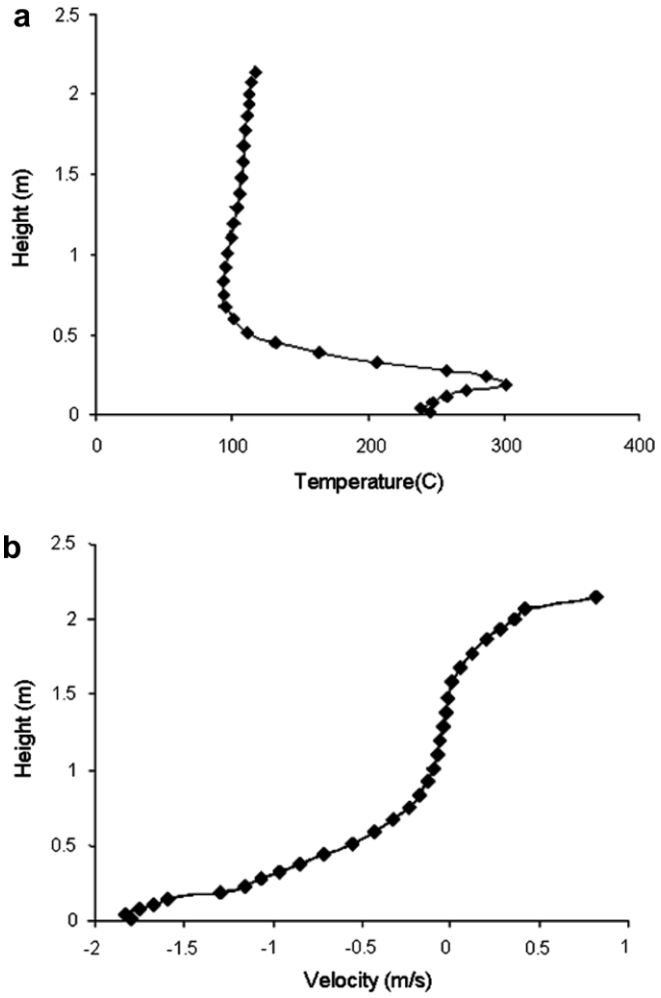


**Fig. 6.** Source centreline: (a) temperature; and (b) velocity, located at ($x$ = 1.4 m, $z$ = 1.4 m).

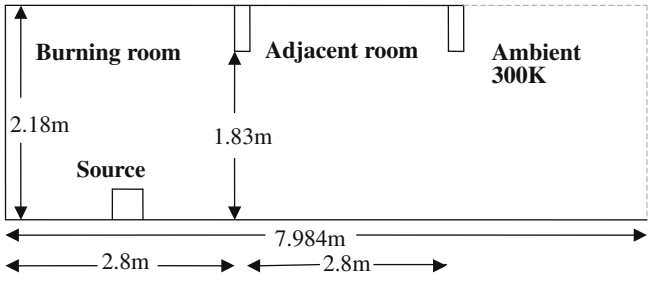


**Fig. 7.** Two-room compartment geometry.

tures within the hot upper layer, thus it provides more accurate prediction of the temperature non-uniformity. It is evident that more research is needed in order to understand which turbulence model performs better, in terms of mass flow rate calculations. However, given that the differences are small, both models may be considered equally suitable, as in the first case. The reported deviations are expected, since the assumptions adopted create uncertainties such as, for example, the omission of the flow rate at the burner. The performance of the turbulence models should also be tested including the mass flow production at the source, although high deviations are expected only for sources of very large heat output [28].

Fig. 8 presents temperature and velocity distributions at the middle longitudinal plane, obtained by the Standard $k$–$\varepsilon$ model. The airflow motion is clearly dominated by buoyancy forces produced around the heat source at the middle of the enclosure, and, as in the first case, it may be described as follows: As air passes across the heat source, its temperature increases, thus its density decreases. Because of the buoyancy forces that arise due to density decrease, the hot air rises towards the top space of the burning room. When the hot layer reaches the right vertical wall it descends and exits through the top of the doorway, while fresh air enters the burning room through the bottom. As hot air passes into the adjacent room the height of the boundary between the hot and cold layer increases, leading to an elevation of the neutral-plane height through the adjacent-room door. The displacement of indoor air by the entering cold air, due to air suction caused by the indoor–outdoor pressure difference, leads to a re-circulation region at the middle of the room. As the entering cold air meets the exiting hot air within the adjacent room, the flow stagnates in the middle of the adjacent room and a new vortex is created. Those two vortices form the boundary between cold and hot air masses and maintain the expected hot upper and cold lower layer throughout the enclosure, as already sketched in Fig. 1(b) of the estimated flow field. It must also be mentioned that the vortex near the left wall, observed in the first case (see Fig. 3(b)), is now absent (Fig. 8(b)).

Temperature and velocity results, through the burning-room doorway, obtained using the Standard $k$–$\varepsilon$ model, for both the enclosures considered, are presented in Fig. 9. It may be concluded that for the two-room problem, the velocity of the entering fresh air into the burning room is greater than the velocity for the case of the single-room problem. It is also seen (Table 1) that the mass outflow rate predicted by both turbulence models (Eqn. 18) is greater than that calculated in the single-room case, due to the neutral-plane height subsidence (and thus the increase of the available outflow surface through the doorway), i.e., the neutral-plane height is now calculated at 0.887 m (see Table 1) using both turbulence models, lower than that occurred in the case of the one-room problem.

Temperature and velocity distributions at the burning-room doorway centreline, as well as at the adjacent-room doorway centreline, are illustrated in Fig. 10. It is seen that there is no significant difference in the velocity predictions by both models, through both openings. This means that both turbulence models similarly predict the bi-directional flow motion, through the openings. However, the RNG model results to higher temperature predictions within the hot upper layer, as was also in the case of the one-room geometry. Temperature differences between the turbulence models are even higher at the burning-room opening (see Fig. 10(b)). The height of the boundary between the hot and cold layers was predicted as being 0.887 m (both models) and 1.146 m (Standard $k$–$\varepsilon$), or 1.131 (RNG $k$–$\varepsilon$) (see Table 1), for the burning room and the adjacent-room doorways, respectively. Thus, the thickness of the hot upper layer in the burning room is greater than the thickness of the upper layer in the adjacent room (Fig. 10(a)); this is expected because of the better air ventilation in the adjacent room.

## 5. Conclusions

The numerical prediction of flow induced by fire in an enclosure during the fire development is of great importance, because it provides data and dictates actions that concern building services (ventilation systems, fire-fighting devices etc.). The knowledge of the fire spread benefits both the building design and the policy making procedures for extinguishing fires.

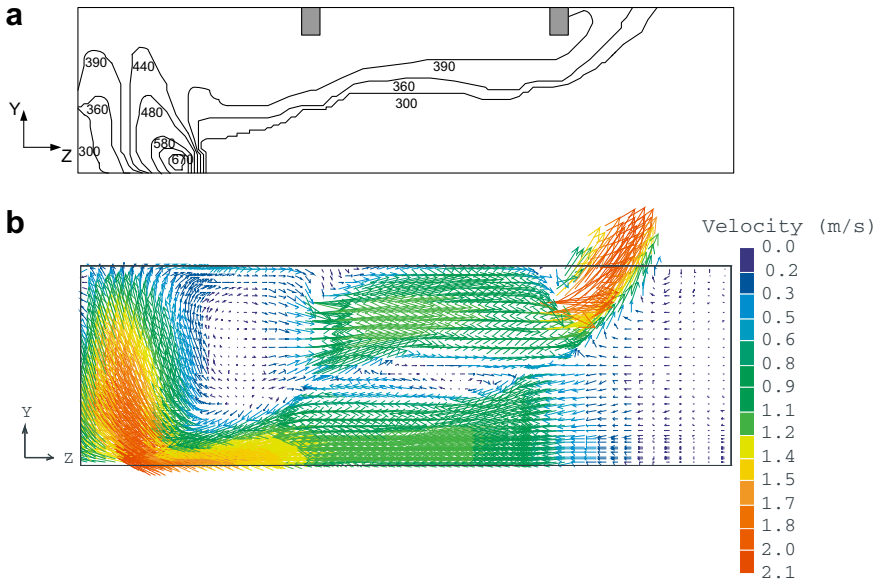


**Fig. 8.** (a) Temperature contours (K); and (b) velocity vectors, at the $y$–$z$ plane at position $x = 1.4$ m.

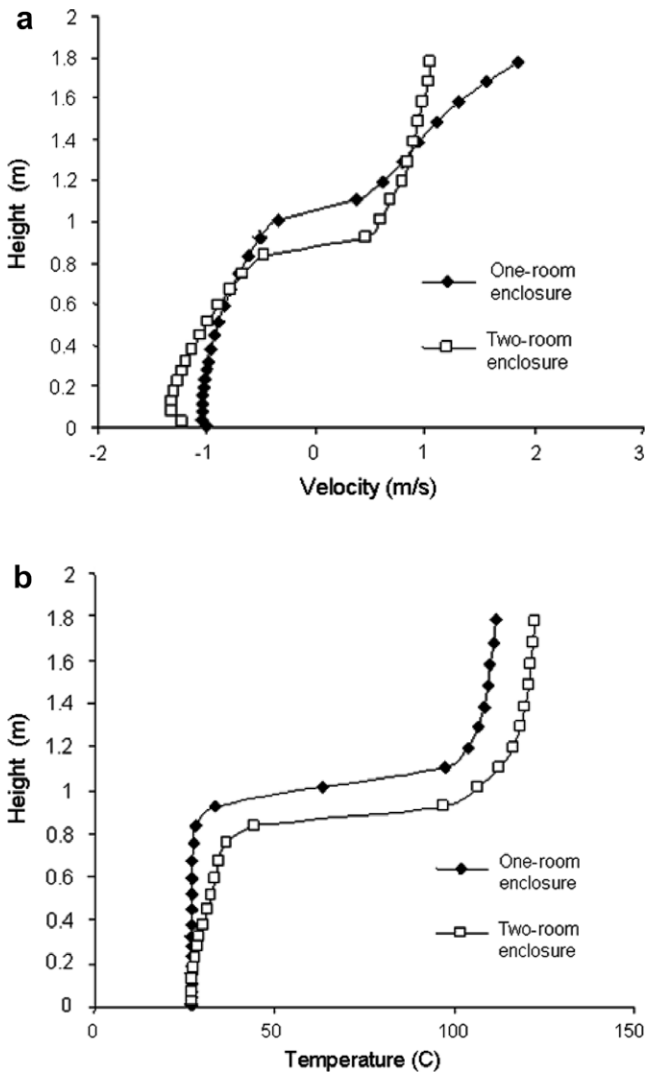


**Fig. 9.** Burning-room doorway centreline: (a) velocity; and (b) temperature, for both one-room and two-room compartments.

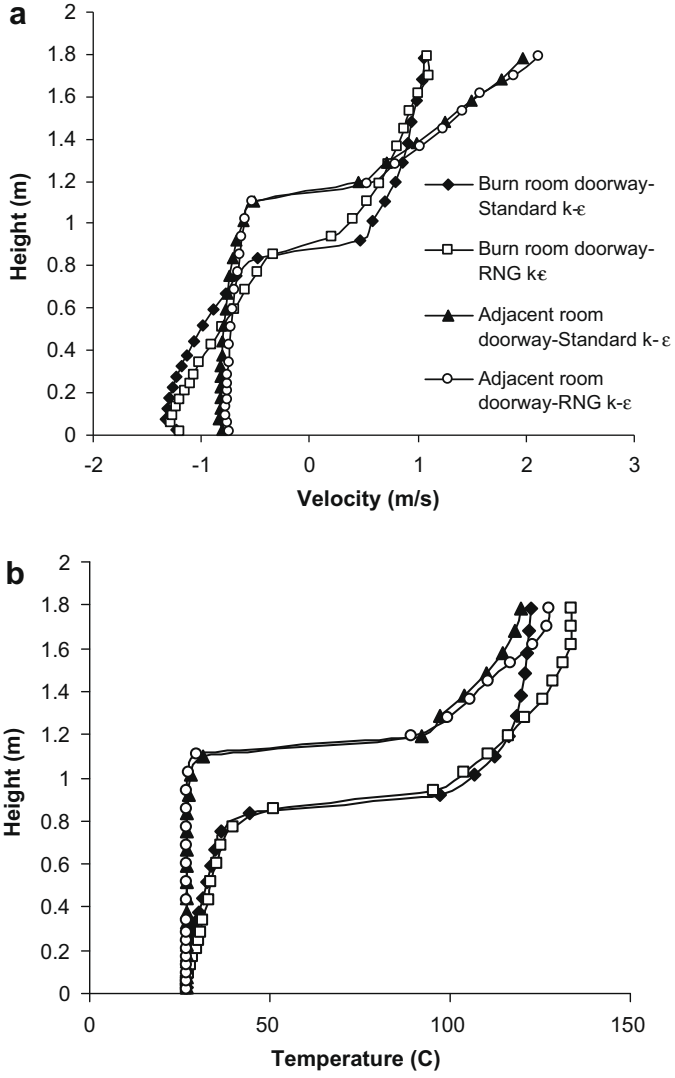


**Fig. 10.** Burning-room and adjacent-room doorway centreline: (a) velocity; and (b) temperature, obtained by both turbulence models.

The objective of the work reported herein was to test two turbulence models against available experimental data and empirical correlations in order to establish the feasibility and practicality of three-dimensional field modelling of strongly buoyant, recirculating flows, for both single- and two-room geometries. A literature review of fire simulation for the above geometries is reported. Significant conclusions of previous studies motivated the present research that focuses on the application of two RANS (Reynolds-Averaged Navier–Stokes) models, i.e., the Standard and the RNG $k$–$\varepsilon$ model, modified to account for buoyancy effects. The results of the first application (single-room problem) appear reasonably accurate, as compared to available experimental data, particularly at the door centreline. Thus, important information for the appropriate design of escape passages in rooms may be provided. The modification of the turbulence models to include the buoyancy effects improved the numerical predictions, but delayed convergence, especially when the RNG model is used. Comparing the two turbulence models, the results appear similar as far as velocity predictions are concerned. The results for temperature, however, differ significantly in the hot upper layer and the RNG model leads to better agreement with the experimental results in this area. The prediction of the hot upper layer height is not affected using either of the two turbulence models. The maximum errors occur at the corner stack of the room, although temperature gradients predicted by the RNG $k$–$\varepsilon$ model are qualitatively similar to those obtained by the experiments. This may be due to the recirculating nature of the flow, which is strong in that area and the logarithmic wall-functions may then be inadequate there. Other treatments should be tested in future to obtain possible improvements of the CFD predictions. However, both models give fairly satisfactory results for engineering purposes. Furthermore, macroscopic design factors, such as the mass outflow rate and the neutral-plane height, are quantitatively predicted by applying a special post-processing procedure consisting of velocity numerical integration through the doorway and regression techniques, respectively. It was found that both turbulence models lead to fair agreement with available mass outflow rate measurements, as well as with those calculated by empirical correlations. Following the aforementioned validation against experiments of the CFD model for the single-room case, the turbulence models were also applied to a two-room geometry and the results obtained are physically plausible. It is observed that both turbulence models predict similar velocity distribution through the openings, while temperature differences occur in the predictions in the hot upper layer, being larger in the burning room. The mass outflow rate and the heights of neutral planes are also calculated at doorways using the numerical results, and thus the thickness of toxic gaseous layers in rooms can be estimated. These predictions are validated against results obtained by well-known empirical correlations, found in literature, and acceptable agreement is obtained. Important information may be provided therefore, with some confidence, for the design of emergency exits and for planning how to extinguish fires, in case of hazardous scenarios caused by residential accidents, in the building pre-construction phase.

In summary, it is concluded that both turbulence models may be used for fire spreading predictions producing similar results, with the RNG $k$–$\varepsilon$ model leading to higher, and more accurate, temperatures above neutral-plane heights. Bi-directional flow through doorways is predicted similarly by both models, in terms of velocity distribution, for both cases studied. Although the well-known deficiencies of the turbulence models used in handling accurately the complicated interactions between fire plume and air-entrainment, intermittency etc. exist, it is satisfying that reasonably accurate results, at least for engineering applications, are obtained within practical computer resources. Hopefully, the methodology described may be useful for validation of new empirical and zone models, and applications for which there are no experimental data available.

## Acknowledgement

This work was sponsored by the Greek National Scholarships Institute.

## References

[1] N.C. Markatos, M.R. Malin, G. Cox, Mathematical modeling of buoyancy-induced smoke flow in enclosures, Int. J. Heat Mass Transfer 25 (1) (1982) 63–75.
[2] N.C. Markatos, G. Cox, Hydrodynamics and heat transfer in enclosures containing a fire source, J. Physicochem. Hydrodyn. 5 (1) (1984) 53–66.
[3] V. Novozhilov, Computational fluid dynamics modeling of compartment fires, Prog. Energy Combust. Sci. 27 (6) (2001) 611–666.
[4] K.B. McGrattan, R.G. Rehm, H.R. Baum, Fire-driven flows in enclosures, J. Comput. Phys. 110 (2) (1994) 285–291.
[5] W.K. Chow, Application of computational fluid dynamics in building services engineering, Build. Environ. 31 (5) (1996) 425–436.
[6] F.W. Mowrer, Enclosure smoke filling and management with mechanical ventilation, Fire Technol. 38 (2001) 33–56.
[7] C.W. Pope, H. Barrow, Theoretical analysis of fluid flow and heat transfer in stoichiometric combustion in a naturally ventilated control volume, Appl. Energy 83 (5) (2006) 464–476.
[8] E. Cui, W.K. Chow, Simulation on indoor aerodynamics induced by an atrium fire, Build. Environ. 40 (9) (2005) 1194–1206.
[9] G.M. Stavrakakis, M.K. Koukou, M.Gr. Vrachopoulos, N.C. Markatos, Natural cross-ventilation in buildings: building-scale experiments, numerical simulation and thermal comfort evaluation, Energy Build. 40 (9) (2008) 1666–1681.
[10] M.L. Janssens, H.C. Tran, Data reduction of room tests for zone model validation, J. Fire Sci. 10 (1992) 528–555.
[11] G. Cox, S. Kumar, N.C. Markatos, Some field model validation studies, in: Fire Safety Science-Proceedings of the First International Symposium, Hemisphere Publishing, 1986, pp. 159–171.
[12] N.C. Markatos, K.A. Pericleous, An investigation of three-dimensional fires in enclosures, Rev. Gen. Thermique 23 (266) (1984) 66–78.
[13] K.D. Steckler, J.G. Quintiere, W.J. Rinkinen, Flow induced by fire in a compartment, National Bureau of Standards, Center for Fire Research, NBSIR, 82-2520, 1982.
[14] W.K. Chow, Application of computational fluid dynamics in building services engineering, Build. Environ. 31 (5) (1996) 425–436.
[15] D.B. Spalding, Mathematical modelling of fluid mechanics, heat transfer and chemical reaction processes, Computational Fluid Dynamics Unit Report No. HTS/80/1, Imperial College of Science and Technology, London, 1980.
[16] M.J. Lewis, M.B. Moss, P.A. Rubini, CFD modelling of combustion and heat transfer in compartment fires, in: Proceedings of the 5th International Symbosium on Fire Safety Science, IAFSS, 1997, pp. 463–474.
[17] B.F. Magnussen, B.H. Hjertager, On mathematical models of turbulent combustion with special emphasis on soot formation and combustion, in: Proceedings of 16th International Symposium on Combustion, Cambridge, MA, 1976, pp. 719–729.
[18] H. Xue, J.C. Ho, Y.M. Cheng, Comparison of different combustion models in enclosure fire simulation, Fire Safety J. 36 (1) (2001) 37–54.
[19] F. Liu, J.X. Wen, The effect of turbulence modelling on the CFD simulation of buoyant diffusion flames, Fire Safety J. 37 (2) (2002) 125–150.
[20] R. Hasib, R. Kumar, Shashi, S. Kumar, Simulation of an experimental compartment fire by CFD, Build. Environ. 42 (9) (2007) 3149–3160.
[21] W.K. Chow, J. Li, Numerical simulations on thermal plumes with $k$–$\varepsilon$ types of turbulence models, Build. Environ. 42 (8) (2007) 2819–2828.
[22] G. Gan, Prediction of turbulent buoyant flow using an RNG $k$–$\varepsilon$ model, Num. Heat Transfer A 33 (1998) 169–189.
[23] D. Morvan, B. Portiere, M. Larini, J.C. Loraud, Numerical simulation of turbulent diffusion flame in cross flow, Combust. Sci. Technol. 140 (1998) 93–122.
[24] I. Nakaya, T. Tanaka, M. Yoshida, Doorway flow induced by a propane fire, Fire Safety J. 10 (3) (1986) 185–195.
[25] C. Nielsen, C. Fleischmann, An analysis of pre-flashover fire experiments with field modelling comparisons, Fire Engineering Research Report, ISNN 1173-5996, University of Canterbury, NZ, 2000.
[26] L. Rutherford, Experimental results for pre-flashover fire experiments in two adjacent ISO compartments, MSc thesis, University of Canterbury, New Zeland, 2002.
[27] G.H. Yeoh, R.K.K. Yuen, E.W.M. Lee, S.C.P. Chueng, Fire and smoke distribution in a two-room compartment structure, Int. J. Num. Meth. Heat Fluid Flow 12 (2) (2002) 178–194.
[28] W.K. Chow, G.W. Zou, Correlation equations on fire-induced air flow rates through doorway derived by large eddy simulation, Build. Environ. 40 (7) (2005) 897–906.
[29] G.H. Yeoh, R.K.K. Yuen, S.M. Lo, D.H. Chen, On numerical comparison of enclosure fire in a multi-compartment building, Fire Safety J. 38 (1) (2003) 85–94.

[30] V. Babrauskas, R.D. Peacock, Heat release rate: the single most important variable in fire hazard, Fire Safety J. 18 (3) (1992) 255–272.
[31] H.K. Versteeg, W. Malalasekera, An introduction to computational fluid dynamics, The Finite Volume Method, Longman Scientific & Technical Ltd, Essex, England, 1995. pp. 10–27.
[32] C. Pozrikidis, Fluid dynamics: theory, Computation and Numerical Simulation, Kluwer academic publishers, Norwell, Massachusetts, USA, 2001. pp. 50–110.
[33] S.V. Patankar, D.B. Spalding, A calculation procedure for heat, mass and momentum transfer in parabolic flows, Int. J. Heat Mass Transfer 15 (10) (1972) 1787–1806.
[34] N.C. Markatos, The mathematical modelling of turbulent flows, Appl. Math. Model. 10 (3) (1986) 190–220.
[35] A. Yakhot, S. Orszag, Renormalisation group analysis of turbulence. I. Basic theory, J. Sci. Comput. 1 (1) (1986) 1–51.
[36] N.C. Markatos, K.A. Pericleous, Laminar and turbulent natural convection in an enclosed cavity, Int. J. Heat Mass Transfer 27 (5) (1984) 755–772.
[37] N.C. Markatos, Mathematical modeling of single- and two-phase flow problems in the process industries, Revue de l' Institute Francais du Petrole 48 (6) (1993) 631–662.
[38] B.E. Launder, D.B. Spalding, Mathematical Models of Turbulence, Academic Press, 1972.
[39] R.K.K. Yuen, G.H. Yeoh, D. Chen, A numerical comparison of combustion and heat transfer in compartment fires, in: Proceedings of 2nd International Conference on Advances in Computational Heat transfer (2nd ICHMT), 2001, pp. 349–356.
[40] H.W. Emmons, Vent flows SFPE Handbook of Fire Protection Engineering, in: P.J. Di Nenno (Ed.), Society of Fire Protection Engineers, second ed., Boston, Massachusetts, 1995, pp. 240–249.